Room-Temperature Synthesis of Ultrasmall Sulfur-Free SnO2 Quantum Dots as an Electron Transport Layer in Perovskite Solar Cells

Supplementary material

Gidey, Abraha Tadese; Rad, Elnaz Ghahremani; Latosinsky, Katherine; SURESH, Sunil & Uhl, Alexander R. (2026) Room-Temperature Synthesis of Ultrasmall Sulfur-Free SnO2 Quantum Dots as an Electron Transport Layer in Perovskite Solar Cells. In: Chemistry of Materials,.

DOI: 10.1021/acs.chemmater.6c01064
Handle: http://hdl.handle.net/1942/49533

Supplementary Information

Room-Temperature Synthesis of Ultra-Small Sulfur-Free SnO_2 Quantum Dots as Electron Transport Layer in Perovskite Solar Cells

Abraha Tadese Gidey,[1*] Elnaz Ghahremani Rad,[1] Katherine Latosinsky,[1] Sunil Suresh,[1,2,3,4], and Alexander R. Uhl[1*]

[1]Laboratory for Solar Energy and Fuels (LSEF), School of Engineering, The University of British Columbia, Kelowna V1V 1V7, Canada

[2]Now at: imec, IUMAT, Thor Park 8320, B-3600 Genk, Belgium

[3]Now at: UHasselt, Institute for Materials Research (IUMAT), Martelarenlaan 42, B-3500 Hasselt, Belgium

[4]Now at: EnergyVille, IUMAT, Thor Park 8320, B-3600 Genk, Belgium

*Corresponding authors: abraha.gidey@ubc.ca (A.T.G.) and alexander.uhl@ubc.ca (A.R.U.)

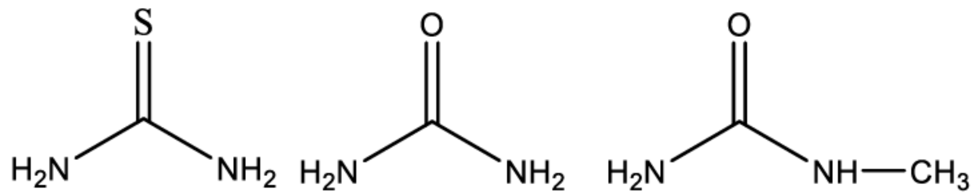

Thiourea (TU) Urea (U) N-methylurea (NMU)

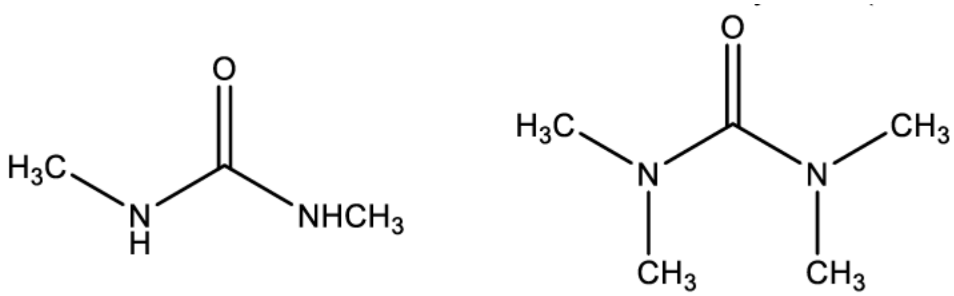

1 3-dimethylurea (DMU) 1,1,3,3-tetramethylurea (TMU)

Figure S1. Chemical structures of the ligands used to synthesize SnO_2 QDs.

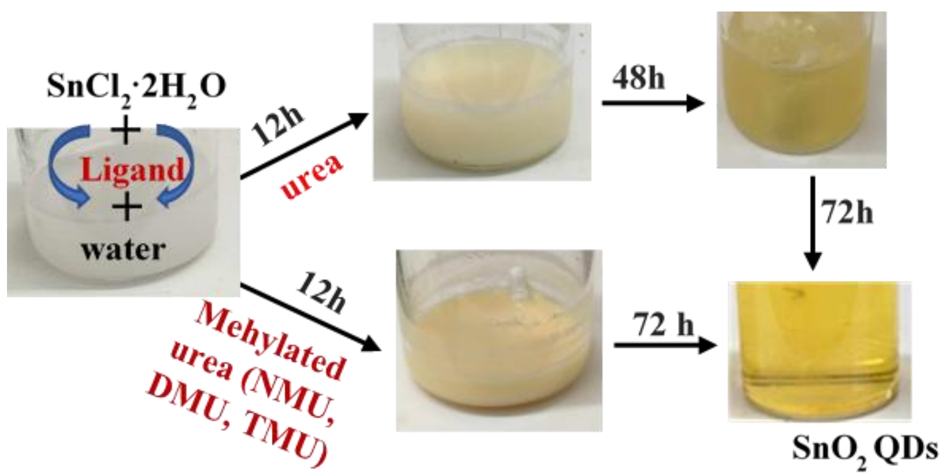

Figure S2. Synthetic pathway of urea and methylated urea-based SnO_2 QDs.

SnO_2 QDs formation processes (synthesis steps provided below).[1]

$SnCl_2 + H_2O \rightarrow Sn(OH)Cl + HCl$ (hydrolysis) (1)

$Sn(OH)Cl + H_2O \rightarrow Sn(OH)_2 + HCl$ (hydrolysis) (2)

$Sn(OH)_2 + O_2 \rightarrow SnO_2 + H_2O$ (dehydration and oxidation) (3)

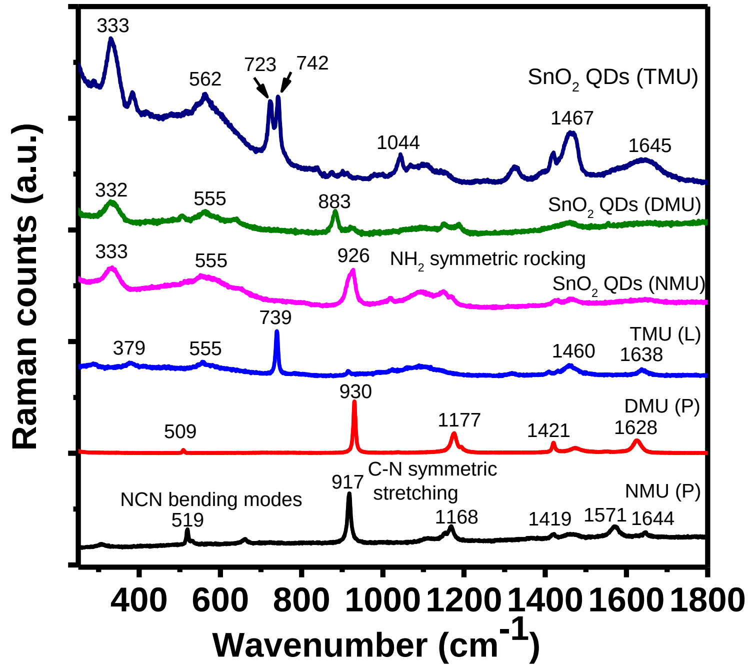

Figure S3. Raman spectra of urea-based ligands and corresponding SnO_2 QDs solutions.

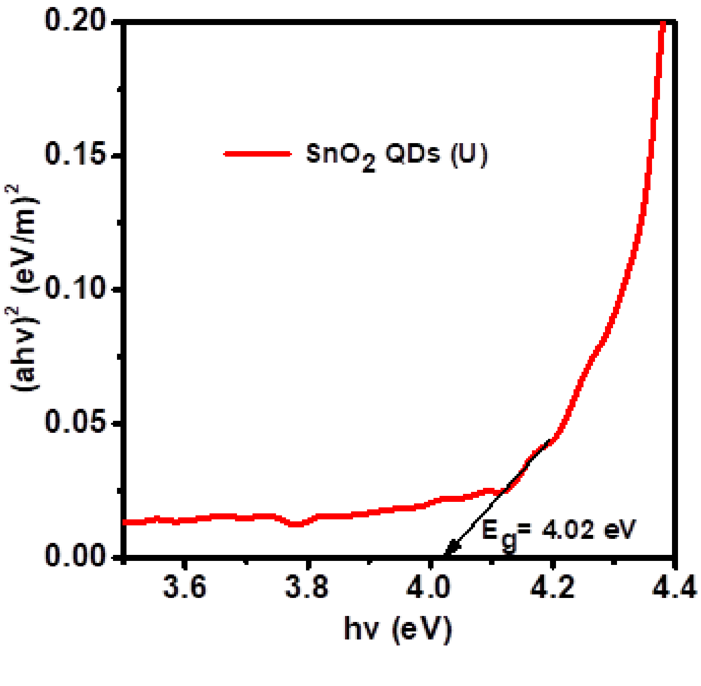

Figure S4. Calculated optical band gap of SnO_2 QD (U).

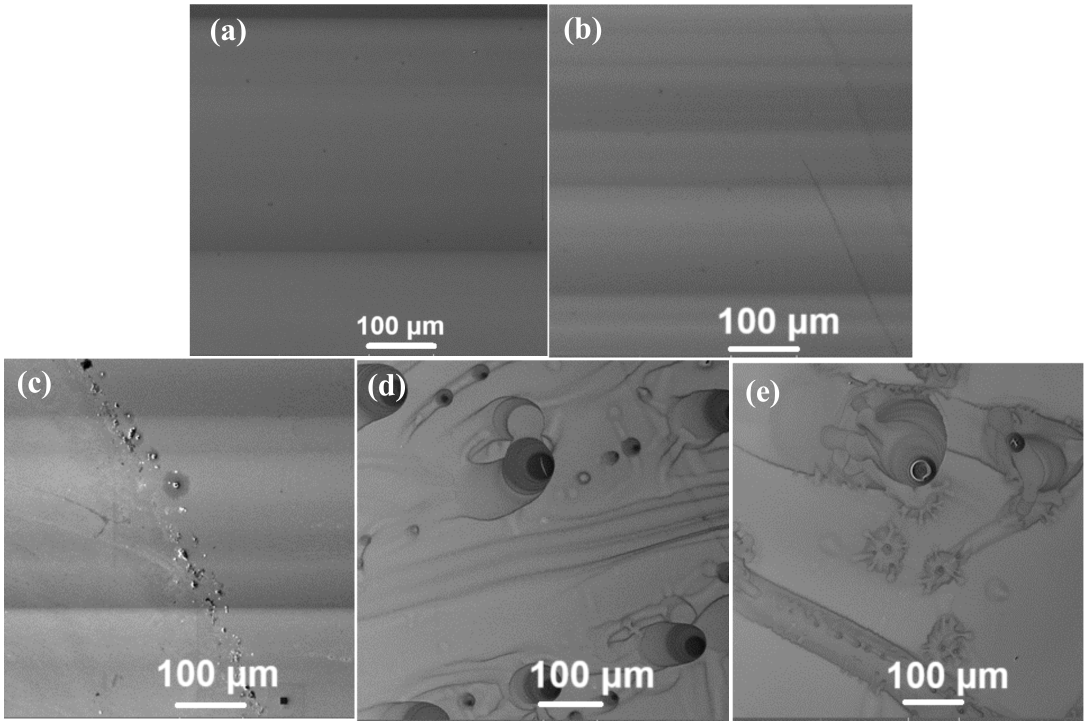

Figure S5. Top-view SEM images at low magnification for SnO_2 QDs derived from (a) thiourea, (b) urea, (c) NMU, (d) DMU, and (d) DMU deposited on FTO.

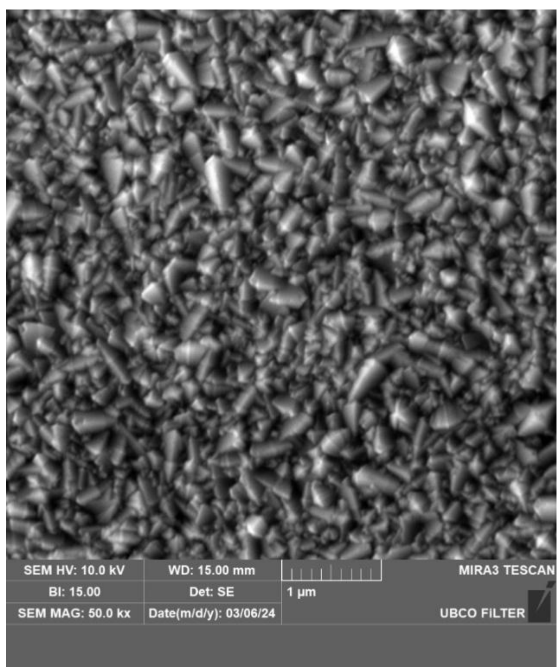

Figure S6. Top-view SEM image of bare FTO.

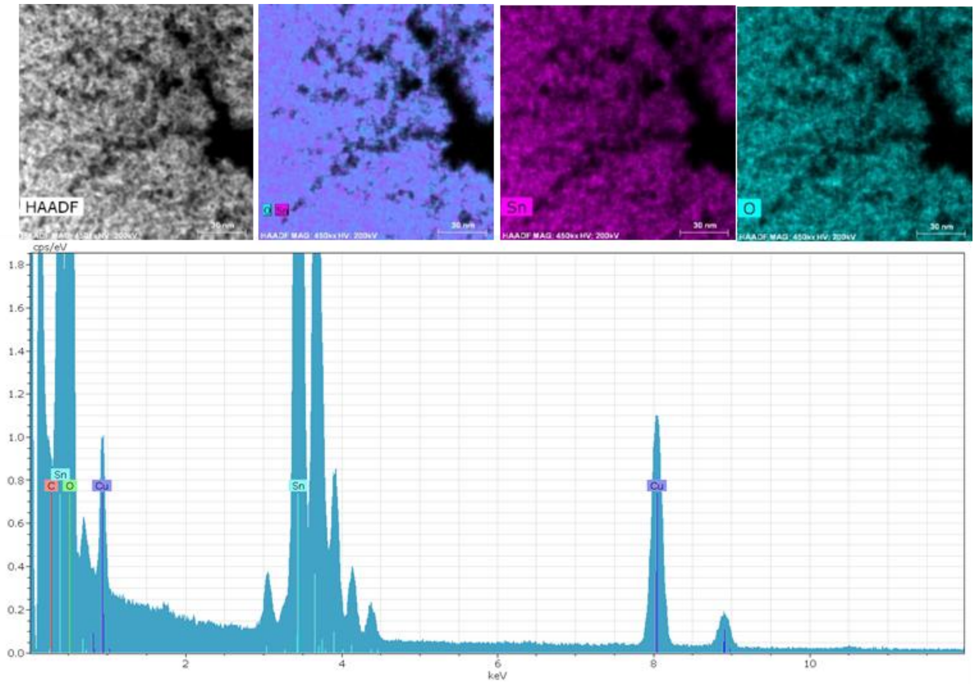

Figure S7. High-angle annular dark-field (HAADF) STEM image maps of SnO_2 (U).

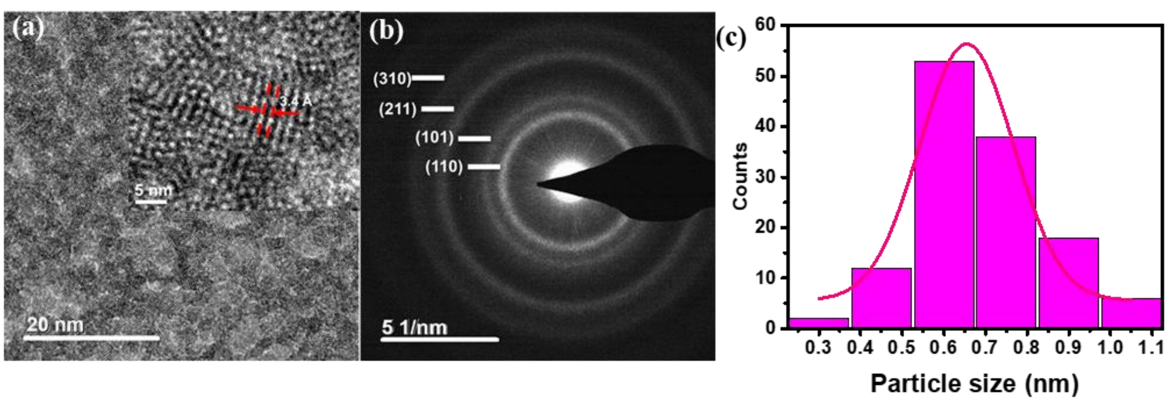

Figure S8. (a)Transmission electron microscopy (TEM) images of SnO_2 QDs (NMU, methylated urea). (b) SAED pattern of SnO_2 QD of SnO_2 QDs (NMU), and (c) particle size distribution of SnO_2 QDs (NMU).

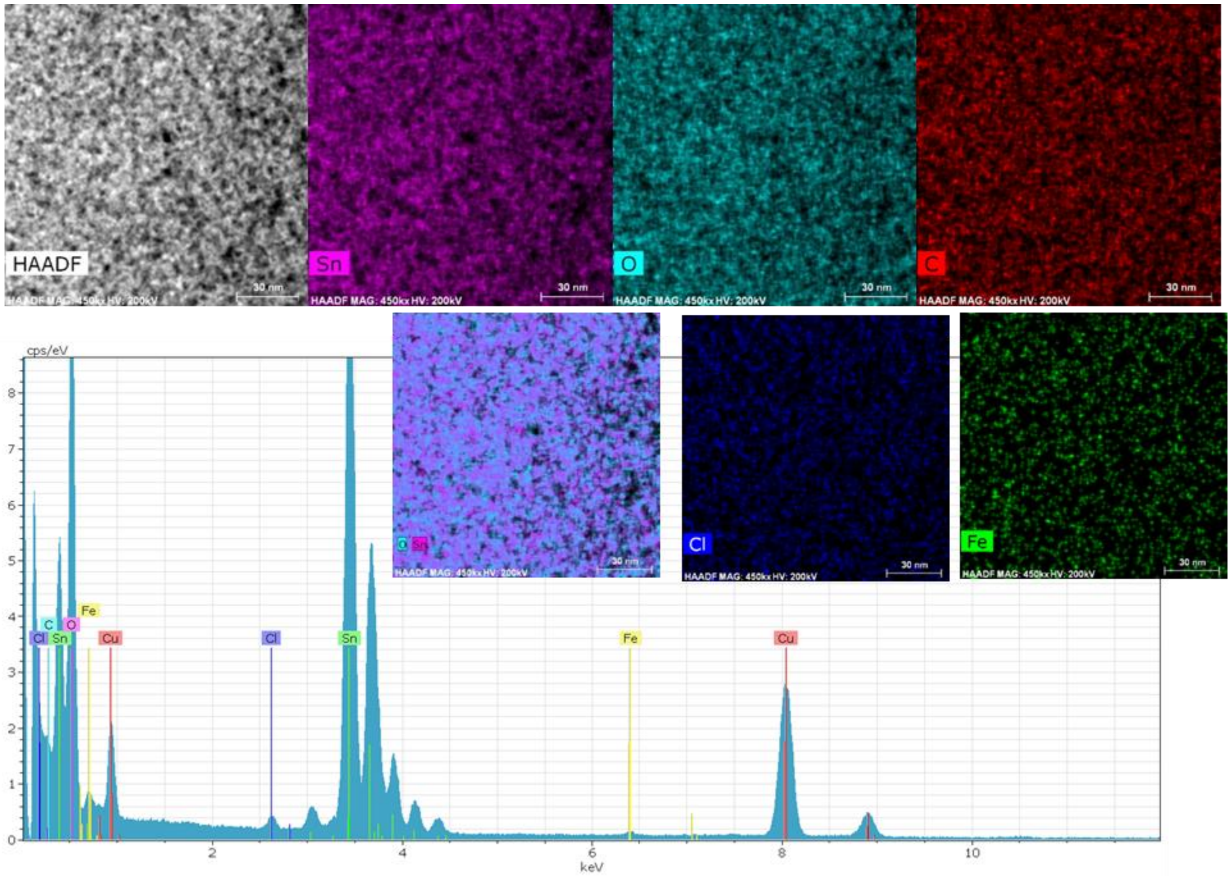

Figure S9. High-angle annular dark-field (HAADF) STEM image maps of SnO_2 (methylated urea (NMU).

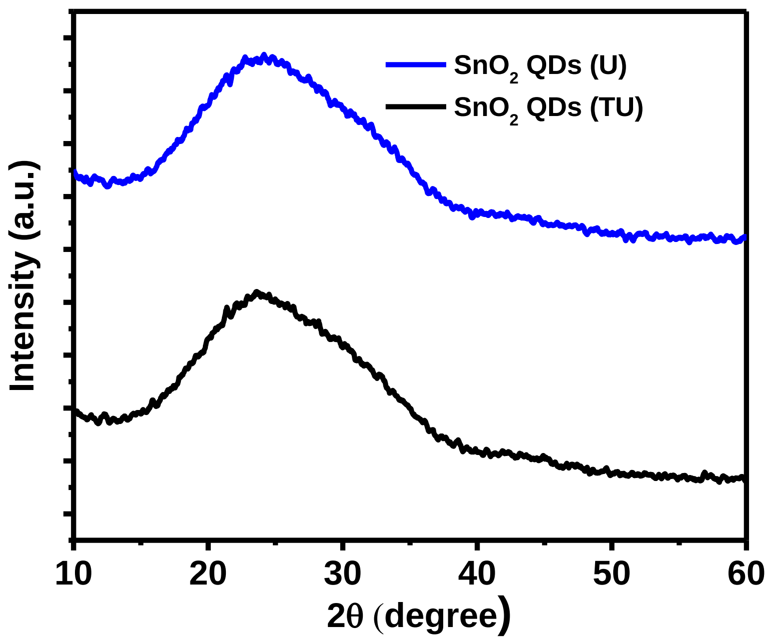

Figure S10. (a) XRD patterns of SnO_2 QDs on glass annealed at 150 ^oC.

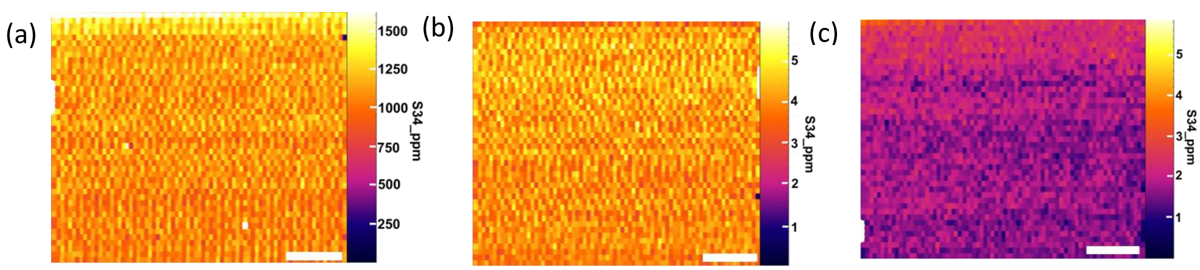

Figure S11. Laser ablation inductively-coupled plasma mass spectrometry (LA-ICP-MS) elemental distribution of S (34S) SnO_2 QDs synthesized from: (a) TU annealed at 150 ^oC, (b) TU annealed at 200 ^oC, and (c) U annealed at 150 ^oC (Scale bar : 200 μm).

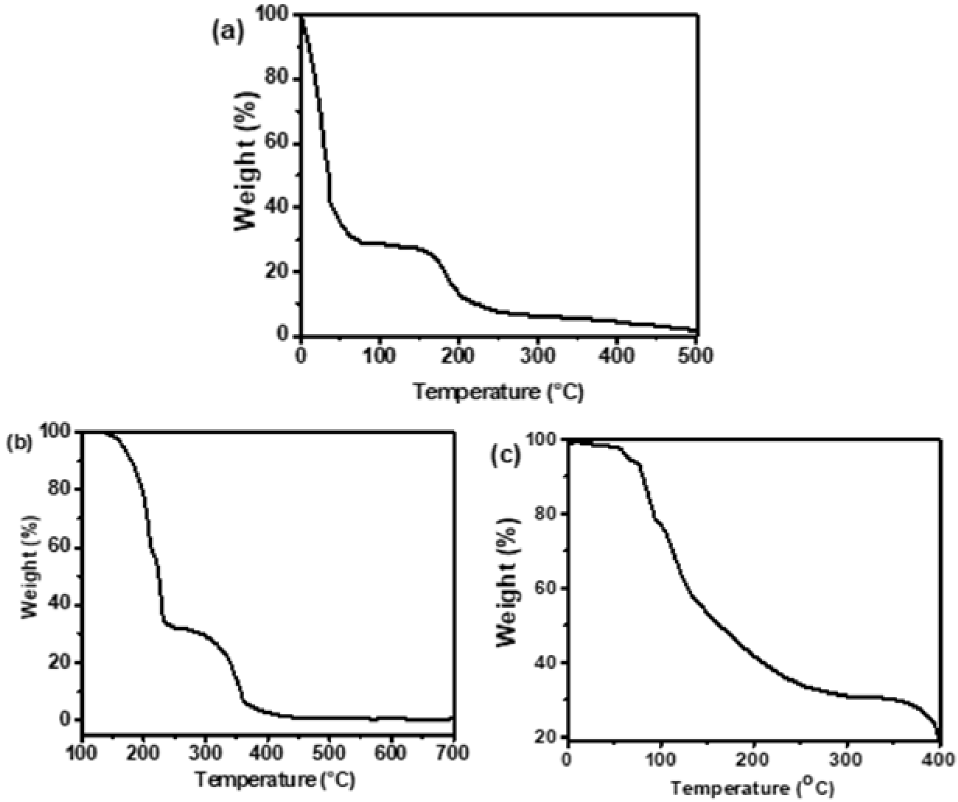

Figure S12. Thermogravimetric analysis (TGA) curves of: (a) thiourea, (b), urea, (c) methylated urea (TMU).[2–4]

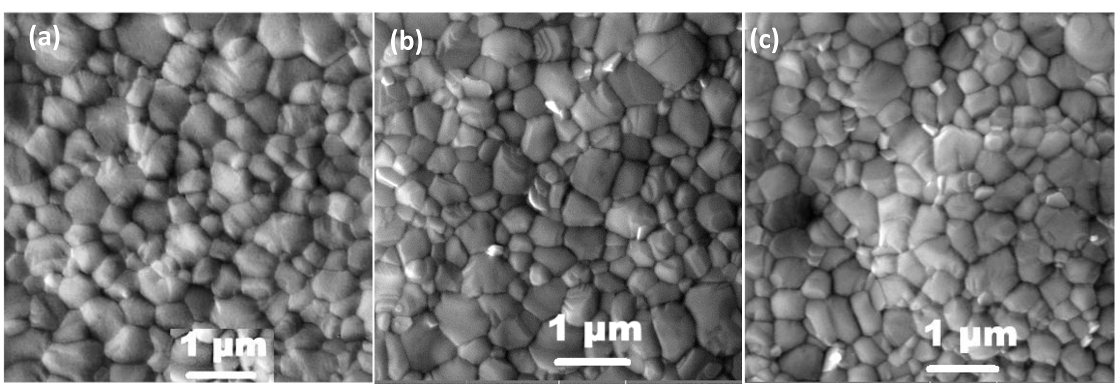

Figure S13. SEM image of $Cs_{0.1}FA_{0.90}PbI_3$ on: (a) SnO_2 QDs thin film (TU), (b) SnO_2 QDs thin film (U), and (c) SnO_2 QDs thin film (methylated, NMU).

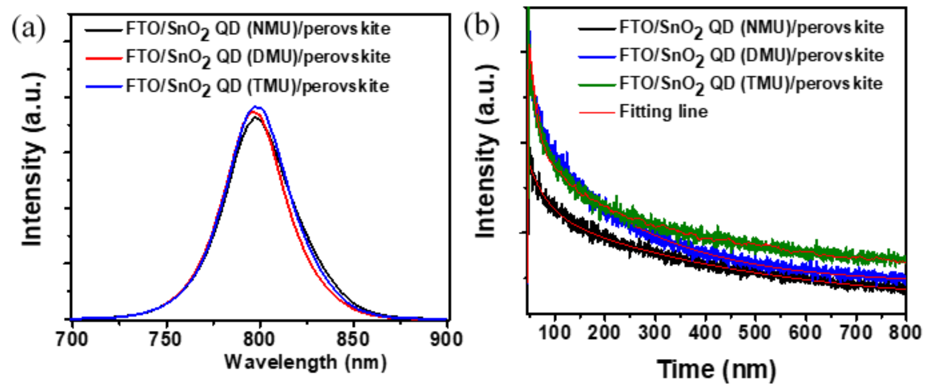

Figure S14. PL spectra of the FTO/SnO_2 QDs /perovskite, and (d) TRPL spectra of the FTO/SnO_2 QDs/perovskite (for the methylated urea-based SnO_2 QDs).

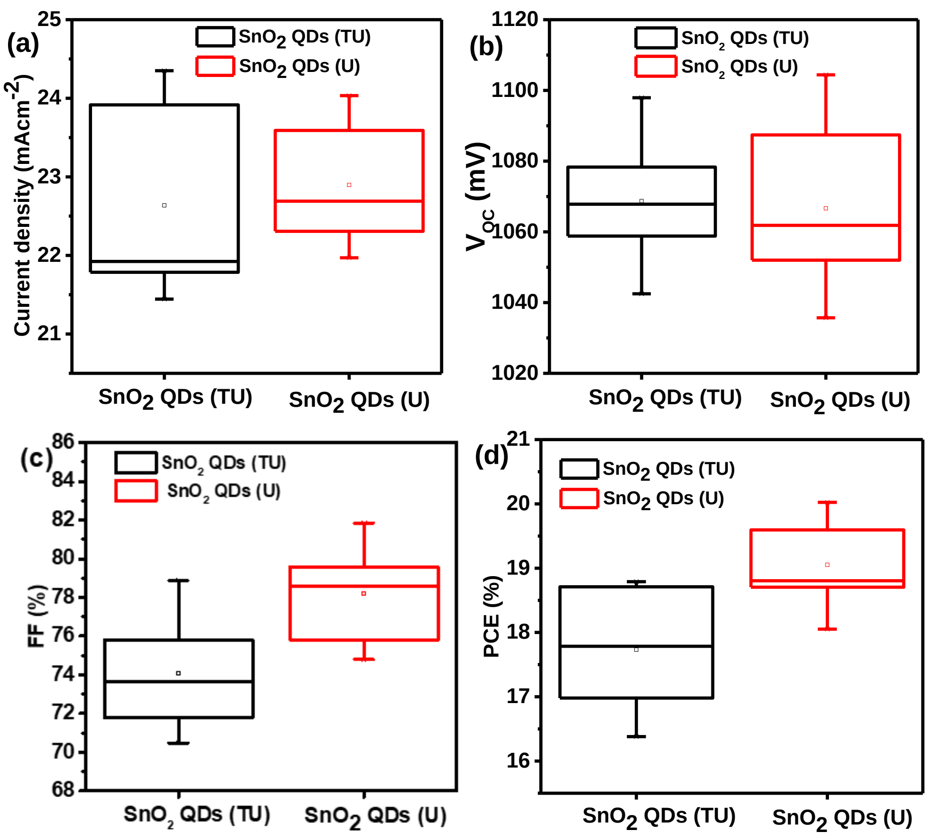

Figure S15. Statistical box plots of the PV parameters obtained from devices using various SnO_2 QDs as ETL: (a) J_{SC}, (b), V_{OC}, (c) FF, and (d) PCE. Boxes show the interquartile range (25th to 75th percentiles), the horizontal line inside boxes show the median, while whiskers show the lowest and highest values.

Table S1: Photovoltaic parameters of PSCs based on the urea-derived SnO_2 QDs ETLs at various annealing temperatures.

Temperature (°C)	**J_{SC} ($mAcm^{-2}$)**	**V_{OC} (mV)**	**FF (%)**	**PCE (%)**
70	20.95±0.58	1027±25.9	74.65±2.89	16.06±0.44
100	21.22±0.43	1078±24.9	75.83±3.20	17.35±0.71
150	22.72±0.70	1079±18.9	78.42±1.92	19.23±0.49
200	21.86±1.02	1068±42.5	77.96±1.06	18.20±0.54

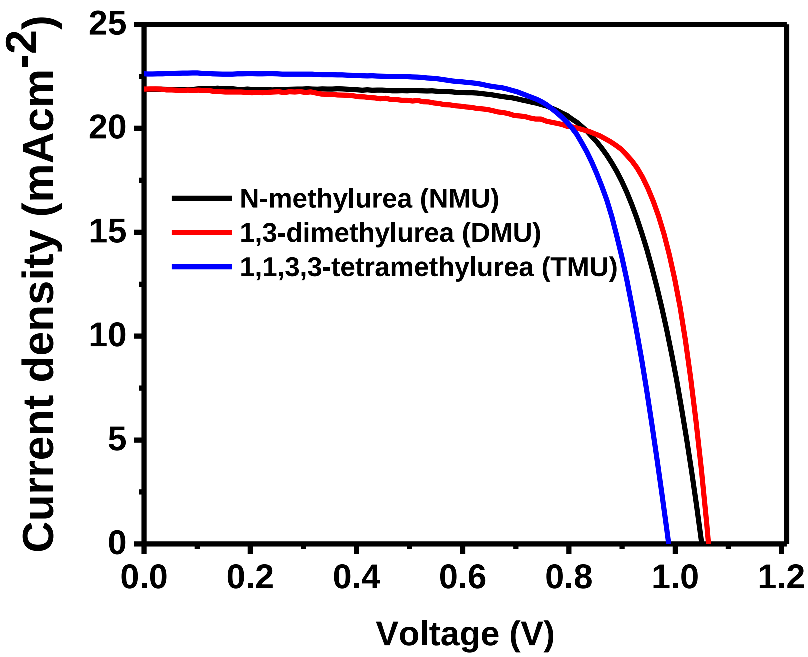

Figure S16. J–V curves of methylated urea-derived SnO_2 QDs-based PSCs.

Table S2: Photovoltaic parameters of PSCs based on SnO_2 QD ETLs (methylated urea, averaged over 10 devices).

SnO_2 QDs	J_{SC} (mAcm^{-2})	V_{OC} (mV)	FF (%)	PCE (%)
SnO_2-NMU	20.91±0.63	1038±25.8	74.58±2.08	16.18±0.31
SnO_2-DMU	20.84±0.72	1037±25.8	74.53±2.88	16.11±0.32
SnO_2-TMU	20.82±0.83	1037±21.9	74.16±1.26	16.00±0.23

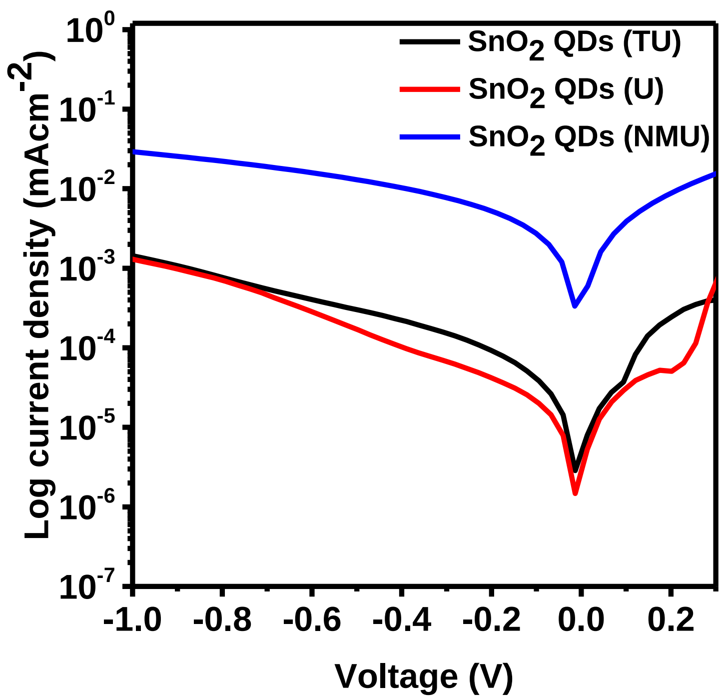

Figure S17. Dark current curves of SnO_2 QD-based PSCs.

Table S3: Photovoltaic comparison and synthetic methods of SnO_2 QDs as ETLs in PSCs (room temperature ink synthesis indicated with (r.t.)

Device structure	Synthetic Method	V_{OC} (mV)	J_{SC} ($mAcm^{-2}$)	FF (%)	PCE (%)	Active area (cm^2)	Ref.
FTO/SnO_2 QDs/ SnO_2 NC/$CsMAFAPbI_3Br_{3-x}$/Spiro-OMeTAD/Ag	2-(2-aminoethyl) isothiourea dihydrobromide (r.t)	1.19	24.75	78.20	23.00	0.04	[1]
ITO/SnO_2 QDs /$(Cs_{0.05}(FA_{0.83}MA_{0.17})_{0.95}$ $Pb(I_{0.83}Br_{0.17})_3$ spiro-OMeTAD/ Au	CH_4N_2S reaction (r.t.)	1.09	19.50	78.00	16.60	0.1	[6]
FTO/SnO_2 QDs /$(FAPbI_3)_{0.875}(CsPbBr_3)_{0.125}$/spiro-OMeTAD/ Au	CH_4N_2S reaction (r.t.)	1.10	23.02	77.50	19.80	1.0	[7]
FTO/TiO_2/SnO_2 QDs/$CsMAFAPbI_3Br_{3-x}$/Spiro-OMeTAD/Au	CH_4N_2S reaction (r.t.)	1.11	20.70	75.30	17.31	0.09	[8]
FTO/SnO_2 QDs/$CH_3NH_3PbI_3$/Spiro-OMeTAD/Ag	CH_4N_2S reaction (r.t.)	1.06	21.60	74.61	17.01	NA	[9]
FTO/SnO_2 QDs/ SnO_2 NC/$CsMAFAPbI_3Br_{3-x}$/Spiro-OMeTAD/Ag	CH_4N_2S reaction (r.t.)	1.08	23.05	81.63	20.32	0.04	[10]
FTO/SnO_2 QDs/$CH_3NH_3PbI_3$/Spiro-OMeTAD/MoO_x/Al	solvothermal technique	0.99	18.80	69.00	12.90	0.1	[11]
ITO/SnO_2/SnO_2 QDs/$MAPbI_3$/ carbon	CTAB (r.t.)	0.85	19.77	70.00	11.76	NA	[12]
FTO/SnO_2/ QDs/$MAPbI_3$/Spiro-OMeTAD/Ag	Microwave-assisted	1.14	23.38	76.20	20.24	NA	[13]

FTO/SnO_2/ QDs/ $MAPbI_3)_{0.7}(FAPbI_3)_{0.3}$/Spiro-OMeTAD/Au	solution processing	1.08	23.40	74.00	18.80	0.09	[14]
FTO/SnO_2 QDs/ $CS_{0.1}FA_{0.9}PbI_3$/Spiro-OMeTAD/Ag	$CO(NH_2)_2$ reaction (r.t.)	1.04	23.60	81.85	20.01	0.16	This work

REFERENCES

(1) Ren, Z.; Liu, K.; Hu, H.; Guo, X.; Gao, Y.; Fong, P. W. K.; Liang, Q.; Tang, H.; Huang, J.; Zhang, H.; et al. Room-Temperature Multiple Ligands-Tailored SnO_2 Quantum Dots Endow in Situ Dual-Interface Binding for Upscaling Efficient Perovskite Photovoltaics with High V_{OC}. *Light Sci. Appl.* **2021**, *10*, 239.

(2) Ogawa, H.; Sato, Y.; Mori, H. Tetramethylurea Dimer/Lithium Salt-Based Deep Eutectics as a Novel Class of Eutectic Electrolytes. *Mater. Chem. Front.* 2021, *5*, 8078–8085.

(3) Zhang, H.; Xi, Y.; Su, C.; Liu, Z. G. Lab Study of Urea Deposit Formation and Chemical Transformation Process of Diesel Aftertreatment System. In *SAE Technical Papers*; SAE International, **2017**, 2017-01-0915.

(4) Park, S. N.; Sung, S. J.; Son, D. H.; Kim, D. H.; Gansukh, M.; Cheong, H.; Kang, J. K. Solution-Processed Cu_2ZnSnS_4 Absorbers Prepared by Appropriate Inclusion and Removal of Thiourea for Thin Film Solar Cells. *RSC Adv.* 2014, *4*, 9118–9125.

(6) Sannino, G. V.; Gries, T. W.; Wang, Q.; Caso, M. F.; De Maria, A.; Lancellotti, L.; Mercaldo, L. V.; Muñoz-García, A. B.; Pavone, M.; Abate, A.; Delli Veneri, P. Optimizing SnO_2 Quantum Dot Precursor Solutions for Perovskite Solar Cells with Reduced Hysteresis. *Solar RRL* **2024**, *8,*

(7) Yang, G.; Chen, C.; Yao, F.; Chen, Z.; Zhang, Q.; Zheng, X.; Ma, J.; Lei, H.; Qin, P.; Xiong, L.; et al. Effective Carrier-Concentration Tuning of SnO_2 Quantum Dot Electron-Selective Layers for High-Performance Planar Perovskite Solar Cells. *Advanced Materials* **2018**, *30*, 1706023.

(8) Wu, T.; Zhen, C.; Wu, J.; Jia, C.; Haider, M.; Wang, L.; Liu, G.; Cheng, H. M. Chlorine Capped SnO_2 Quantum-Dots Modified TiO_2 Electron Selective Layer to Enhance the Performance of Planar Perovskite Solar Cells. *Sci. Bull. (Beijing).* **2019**, *64*, 547–552.

(9) Wang, E.; Chen, P.; Yin, X.; Wu, Y.; Que, W. Tailoring Electronic Properties of SnO_2 Quantum Dots via Aluminum Addition for High-Efficiency Perovskite Solar Cells. *Solar RRL* **2019**, *3, 1900041*.

(10) Luo, Z.; Du, G.; Yang, L.; Zhang, J. Unveiling the Dimensional Effects of SnO_2 Quantum Dots and Nanoparticles on the Interfacial Properties of Perovskite Solar Cells. *J. Power Sources* **2023**, *568*, 232928.

(11) Kiani, M. S.; Parkhomenko, H. P.; Mangrulkar, M.; Aigarayeva, S.; Akhanuly, A.; Shalenov, E. O.; Ng, A.; Jumabekov, A. N. Stepping toward Portable Optoelectronics with SnO_2 Quantum Dot-Based Electron Transport Layers. *ACS Omega* **2023**, *8*, 21212–21222.

(12) Youssef, R. M.; Salem, A. M. S.; Shawky, A.; Ebrahim, S.; Soliman, M.; Abdel-Mottaleb, M. S. A.; El-Sheikh, S. M. Solution-Processed Quantum Dot SnO_2 as an Interfacial Electron Transporter for Stable Fully-Air-Fabricated Metal-Free Perovskite Solar Cells. *Journal of Materiomics* **2022**, *8*, 1172–1183.

(13) Xu, Z.; Jiang, Y.; Li, Z.; Chen, C.; Kong, X.; Chen, Y.; Zhou, G.; Liu, J. M.; Kempa, K.; Gao, J. Rapid Microwave-Assisted Synthesis of SnO_2 Quantum Dots for Efficient Planar Perovskite Solar Cells. *ACS Appl. Energy Mater.* 2021, *4*, 1887–1893.

(14) Liu, H.; Chen, Z.; Wang, H.; Ye, F.; Ma, J.; Zheng, X.; Gui, P.; Xiong, L.; Wen, J.; Fang, G. A Facile Room Temperature Solution Synthesis of SnO_2 Quantum Dots for Perovskite Solar Cells. *J. Mater. Chem. A Mater.* **2019**, *7*, 10636–10643.